frontiers | Frontiers in Built Environment

TYPE Original Research
PUBLISHED 28 August 2025
DOI 10.3389/fbuil.2025.1629114

OPEN ACCESS

EDITED BY
Min Zhou,
North University of China, China

REVIEWED BY
Nuo Duan,
Energie Baden-Württemberg, Germany
Nadhim Hamah Sor,
University of Garmian, Iraq

*CORRESPONDENCE
Wanpeng Shi,
ctswp@mail.scut.edu.cn

RECEIVED 15 May 2025
ACCEPTED 10 July 2025
PUBLISHED 28 August 2025

CITATION
Hou Z, Li G and Shi W (2025) A prediction model for the calculation of effective stiffness of circular hollow reinforced concrete piers. *Front. Built Environ.* 11:1629114. doi: 10.3389/fbuil.2025.1629114

A prediction model for the calculation of effective stiffness of circular hollow reinforced concrete piers

Zequn Hou[1], Guiqian Li[2] and Wanpeng Shi[3]*

[1]Guangxi Communications Design Group Co., Ltd, Nanning, China, [2]Guangxi Vocational and Technical College of Communications, Nanning, China, [3]School of Civil Engineering and Transportation, South China University of Technology, Guangzhou, Guangdong, China

To develop a more rational and practical model for estimating the effective stiffness (ES) of circular hollow reinforced concrete piers (CHRCPs), this study compiled a database of 50 quasi-static tests on CHRCPs exhibiting flexural failure, covering axial load ratios of 0.05–0.3, longitudinal reinforcement ratios of 1.0%–5.4%, shear-span ratios of 2.5–6.1, and hollowness ratios of 0.25–0.77. The applicability of existing reinforced concrete piers ES models to CHRCPs was systematically evaluated. Key influencing parameters the ES of CHRCPs were identified and quantified using a simplified three-component yield displacement model. Meanwhile, a new regression-based model was proposed and calibrated through parametric analysis. The model's accuracy was validated by simulating the lateral force–displacement responses of one full-scale and one scaled CHRCPs. The results demonstrate that, most existing ES models significantly overestimate the ES of CHRCPs, with mean calculated-to-experimental stiffness ratios ranging from 1.41 to 3.68 and coefficients of variation (CVs) of 0.25–0.41. The ES of CHRCPs increases with the axial load ratio, longitudinal reinforcement ratio, and shear-span ratio but decreases with the hollowness ratio. The interaction between shear-span and hollowness ratios was effectively captured via an equivalent shear-span ratio. The proposed model achieves a mean calculated-to-measured stiffness ratio of 1.04 with a CV of 0.21, indicating significantly improved accuracy and reduced dispersion. The proposed model showed good applicability to 11 round-ended hollow piers, achieving a mean stiffness ratio of 0.976 and a mean relative error of 14%, outperforming existing models.

KEYWORDS

reinforced concrete, circular hollow pier, effective stiffness, hollow ratio, regression analysis

1 Introduction

The effective stiffness (ES) of bridge piers plays a critical role in determining the fundamental vibration periods and dynamic responses (lateral deflection and internal force) during seismic analysis. Variations in stiffness significantly affect the yield displacement of bridge piers, which in turn influences displacement ductility demands in nonlinear seismic evaluations. Therefore, accurately estimating the ES of reinforced concrete (RC) bridge piers is essential for reliable seismic performance

assessment of bridge structures (Yukio et al., 1986). Circular hollow reinforced concrete piers (CHRCPs) are widely adopted in bridge engineering due to their high sectional efficiency and favorable seismic behavior (Zahn et al., 1990; Yeh et al., 2001; Lee et al., 2015; Li et al., 2020). However, despite their prevalence, dedicated studies focusing on the ES of CHRCPs remain extremely limited. Given the unique geometric and mechanical characteristics of CHRCPs, it is necessary to systematically investigate the ES of CHRCPs for the accurate seismic assessment of bridge structures subjected to ground motion.

To date, no consensus has been reached among researchers or international design codes regarding the definition and estimation methods for the ES of RC columns. The variation of ES with the design axial load ratio has already been recognized, as noted in FEMA 356 (2000), ASCE 41-06 (2007), ACI 318-19 (2019), Paulay and Priestley (1992), and Kumar and Singh (2010). Meanwhile, these parameters (i.e., axial load ratio, shear-span ratio (Haselton et al., 2008; Elwood and Eberhard, 2009; Berry et al., 2008; Zheng and Li, 2013; Wei et al., 2019), longitudinal reinforcement ratio (Berry et al., 2008; Zheng and Li, 2013), and $f_y d_b/L$ (Zheng and Li, 2013; Wei et al., 2019)) have been identified to govern the ES through theoretical analysis and quasi-static test results of RC columns. Based on the considerations of combinations of these governing parameters, some simplified models were proposed to estimate the ES of RC columns (Haselton et al., 2008; Elwood and Eberhard, 2009; Berry et al., 2008; Zheng and Li, 2013; Wei et al., 2019). In addition, the bending stiffness of column sections derived from moment–curvature analysis was suggested as the ES of bridge piers based on building codes, including China JTG/T2231-01-2020 (referred to hereafter as JTG) (JTG/T2 231-01-2020, 2008), Caltrans (2019), Eurocode 8 (2005), and AASHTO (2015). In recent years, machine learning techniques have also been applied to develop predictive models of concrete column ES (Wang et al., 2022; Sourav and Satyabrata, 2020). However, these data-driven models often lack physical interpretability and require large volumes of training data, limiting their practical engineering applicability.

Most of the aforementioned models have been developed for solid RC piers. Only a model proposed by Wei et al. (2019) was directed against the rectangular hollow piers. Insufficient attention has been paid to the ES of CHRCPs, which are widely used in the bridge engineering field. Meanwhile, applying models developed for hollow and solid RC piers to CHRCPs is problematic, primarily due to the distinct mechanical behavior and confinement effects explored in hollow sections (Liang and Sritharan, 2018; Liang and Sritharan, 2019). Specifically, hollow RC piers tend to exhibit lower effective stiffness and more pronounced shear effects than their solid counterparts of similar dimensions (Sun et al., 2013). While numerous studies have investigated the seismic performance of CHRCPs [2–5、25–35], research directly addressing their ES remains scarce.

This work proposes a more rational, practical, and accurate simplified model to estimate the ES of CHRCPs. The objectives and structure of the article are as follows: Section 2 of this manuscript presents the key innovations. Section 3 defines effective flexural stiffness and ES, clarifying their distinctions and interrelations. Ten existing models for assessing the ES of pier are evaluated in Section 4 based on the data of 50 CHRCPs. Section 5 investigates the main influencing factors for the ES of CHRCPs based on a simplified three-component yield displacement model and experimental data. In Section 6, a new ES model for CHRCPs is developed, calibrated by multiple linear regression, and compared with the existing ES models. Section 7 of this manuscript presents the verification of the ES model proposed in this manuscript by simulating the lateral force–displacement curves of the full-scale and scaled piers and estimating the ES of round-ended hollow piers widely used in railway bridges in China. Finally, Section 8 summarizes the main findings and conclusions of the study.

2 Novelty of the study

Although numerous ES models have been developed for solid and rectangular hollow reinforced concrete piers, there remains a distinct lack of models specifically tailored to the structural and mechanical characteristics of CHRCPs. This research fills that gap by systematically developing and validating an ES prediction model dedicated to CHRCPs, thereby offering a more reliable analytical tool for evaluating the seismic performance of this commonly used pier type. An innovation in this work is the explicit introduction of the hollowness ratio as a governing parameter in the proposed model. While this parameter has been largely overlooked in prior studies, the results demonstrate its significant influence on stiffness degradation. By incorporating the hollowness ratio into the regression framework, the model successfully captures the unique mechanical behavior of hollow sections and reveals a clear inverse correlation between the hollowness ratio and the pier's effective stiffness. This finding provides a refined understanding of how hollow geometry influences structural response under seismic loading.

In addition to identifying the isolated effects of geometric parameters, this study further investigates the coupling mechanism between the shear-span ratio and hollowness ratio, two parameters that jointly influence shear deformation behavior. By establishing a simplified three-component yield displacement model, the research reveals and quantifies their interactive effects. To effectively characterize this relationship, the concept of an equivalent shear-span ratio coefficient is proposed, allowing for a more accurate representation of shear-related stiffness contributions in hollow piers. The applicability of the proposed model is extended beyond standard circular hollow sections to include round-ended hollow piers, which are prevalent in railway bridge engineering. Validation against experimental and numerical data confirms that the model maintains high predictive accuracy for these configurations, significantly outperforming existing models in terms of reliability and generalizability. This extension demonstrates the model's robustness across a range of geometries commonly encountered in practice.

Through rigorous mechanical derivation, parametric analysis, and experimental verification, this study establishes a new analytical framework for assessing the effective stiffness of CHRCPs. The proposed model not only overcomes critical shortcomings of previous approaches but also enhances the precision of seismic analysis and design for bridge structures incorporating circular or round-ended hollow piers.

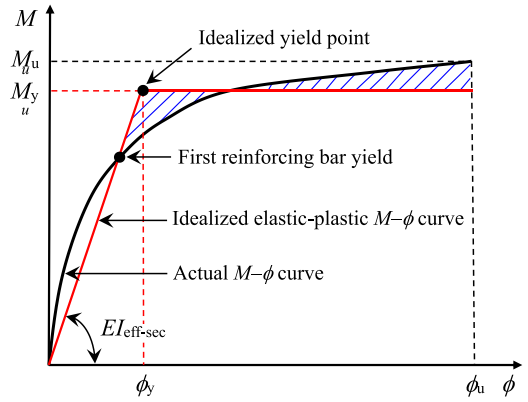

FIGURE 1
Definition of effective section stiffness (JTG/T2 231-01-2020, 2008).

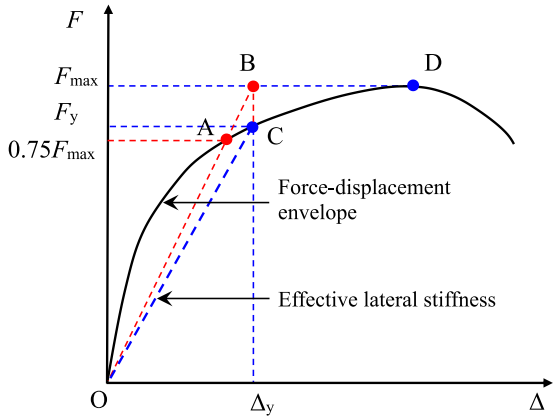

FIGURE 2
Definition of effective stiffness in the proposed method by Park (1989).

3 Definition of ES of bridge piers

3.1 Effective flexural stiffness

Under gravity loading, the cracking of RC bridge piers is typically minor and can generally be neglected, assuming gross-section stiffness is both reasonable and sufficient. However, most RC piers either reach or approach yielding, leading to significant cracking and stiffness degradation under strong seismic excitations. Therefore, it is crucial to consider the realistic stiffness of bridge piers in seismic stability analyses. To reflect the cracked state of RC piers during seismic events, major design codes (i.e., China JTG (JTG/T2 231-01-2020, 2008), Caltrans (2019), Eurocode 8 (2005), and AASHTO (2015)) recommend the use of effective section stiffness in place of gross stiffness. Generally, it can be derived from moment–curvature (M-ϕ) analysis as the effective section stiffness of RC pier and would be determined from secant slope of the idealized elastic–plastic M-ϕ curve between the origin and the idealized yield point as Equation 1 (JTG/T2 231-01-2020, 2008; Caltrans, 2019):

$$EI_{\text{eff-sec}} = \frac{M_y}{\phi_y} \tag{1}$$

where M_y and ϕ_y are the idealized yield moment and yield curvature of the idealized yield point in Figure 1, respectively. This point shall be obtained by balancing the areas between the actual and the idealized M-ϕ curves beyond the first reinforcing bar yield point, as shown in Figure 1.

The rotational degrees of freedom of a pier bottom are assumed to be fixed, and the moment and curvature vary linearly over the height of the pier. Namely, the effective section stiffness is constant over the height of the pier. Hence, the effective section stiffness $EI_{\text{eff-sec}}$ can be regarded as the effective flexural stiffness $EI_{\text{eff-flex}}$.

3.2 ES of bridge piers

There is wide consensus that the estimation of yield displacement and ES for seismic analysis of bridge piers should consider the bending deformation, shear deformation, and bar slip deformation. Therefore, the effective flexural stiffness derived from moment–curvature analysis will overestimate the ES of the bridge pier due to ignoring the influence of shear effect and slip effect. In this study, the ES of bridge piers is defined following the method proposed by Park (1989), based on the measured lateral force–displacement (F-Δ) envelope of the member level. This approach considers the stiffness reduction caused by the shear and slip effect and is considered more representative in capturing the actual yield state of reinforced concrete piers under seismic loading.

As shown in Figure 2, when the force–displacement envelope curve of CHRCPs is known, the detailed procedure for determining its equivalent yield point using Park's method is depicted below. On the ascending branch of the curve, first identify point A corresponding to the lateral force F = 0.75Fmax, where Fmax represents the specimen's maximum lateral force capacity. Point B is then determined as the intersection between line OA (connecting origin O and point A) and the horizontal line passing through point D (the peak point of the backbone curve). The equivalent yield point C (Δ_y, F_y) is finally identified as the intersection between the backbone curve and the vertical line passing through point B. The effective stiffness of CHRCPs can subsequently be calculated using the Δ_y and F_y values from line OC.

In the elastic state, the yield displacement Δ_y and effective stiffness (ES) EI_{eff} of cantilever pier can be defined as (Zheng and Li, 2013).

$$\Delta_y = \frac{F_y \times L^3}{3EI_{\text{eff}}} \tag{2}$$

$$EI_{\text{eff}} = \frac{F_y \times L^3}{3\Delta_y} \tag{3}$$

where L is the equivalent cantilever length of the bridge pier. Here, the EI_{eff} of bridge pier under cyclic lateral loading is taken as the mean value of the positive (push) and negative (pull) directions.

3.3 Relationship between effective section stiffness and ES

It should be noted that the yield displacement obtained from the F-Δ envelope is the sum of the bending deformation, shear deformation, and slip deformation. Then, the assumption that the shear deformation and slip deformation are transformed into equivalent flexural deformation is implicit when calculating the yield displacement of the cantilever pier with Equation 2. Therefore, the ES determined by Equation 3 will be smaller than the effective section stiffness (i.e., effective flexural stiffness) that only considers the bending deformation. Obviously, the factors that affect flexural stiffness also affect ES, and the influencing trend is consistent.

4 Evaluation of existing ES models

4.1 Existing models of ES

In the existing literature (FEMA 356, 2000; ASCE 41-06, 2007; ACI 318-19, 2019; Paulay and Priestley, 1992; Kumar and Singh, 2010; Haselton et al., 2008; Elwood and Eberhard, 2009; Berry et al., 2008; Zheng and Li, 2013; Wei et al., 2019), the ES of concrete columns is generally expressed as a fraction ($EI_{\mathrm{eff}}/E_{\mathrm{c}}I_{\mathrm{g}}$) of the gross-section stiffness $E_{\mathrm{c}}I_{\mathrm{g}}$. Here, E_{c} is the elastic modulus of the concrete, I_{g} is the moment of inertia of the gross section. Based on this, various design specifications and researchers have proposed different models for estimating the ES of RC piers, with 10 representative models summarized in Table 1. In Table 1, models M1–M4 are primarily developed for building structures, while M7–M10 are more relevant to bridge applications. Models M5 and M6 apply to both buildings and bridges. In terms of parameter usage frequency across these models, the most commonly considered variables include axial load ratio, shear-span ratio, longitudinal reinforcement ratio, the normalized reinforcement index $f_{\mathrm{y}}d_{\mathrm{b}}/L\sqrt{f'_{\mathrm{c}}}$, longitudinal reinforcement diameter, and section height.

Notably, M1–M8 were developed for solid-section piers, while model M9 addresses rectangular hollow sections, but the influence of the section hollow ratio is not considered in the M9 model. Therefore, it is necessary to evaluate the applicability and accuracy of existing ES models when applied to CHRCPs.

4.2 Evaluation of existing models

Many studies (Zahn et al., 1990; Yeh et al., 2001; Lee et al., 2015; Li et al., 2020; Whittaker et al., 1987; Unjoh and ASAZU, 1999; Chung et al., 1999; Hoshikuma and Priestley, 2000; Ranzo and Priestley, 2001; Zhu et al., 2009; Kim and Kang, 2012; Kim et al., 2014; Kim et al., 2016; Liang et al., 2021a; Liang et al., 2021b) have provided the quasi-static test data needed to evaluate the accuracy of various ES models to CHRCPs. To limit in the analyses to bridge pier, the selection of test data meets the following requirements: (1) cantilever pier; (2) flexural failure mode; (3) $2.5 \le L/D$; (4) $0.006 \le \rho_{\mathrm{l}} \le 0.06$; (5) $0 \le P/A_{\mathrm{g}}f_{\mathrm{c}}' \le 0.35$; (6) 20 Mpa $\le f_{\mathrm{c}}' \le$50 Mpa, where P is the axial force, A_{g} is the net cross-sectional area of pier, D is the outer diameter of pier, and the meanings of other symbols are the same as before. Based on these criteria, a total of 52 test specimens were selected from the literature. Among them, 50 piers were utilized to evaluate the performance of existing ES models and for calibrating the regression model proposed in this study. The remaining two specimens, named PS1-C (Yeh et al., 2001) and HC-O-100 (Kim and Kang, 2012), were reserved for independent verification of the proposed model.

It should be noted that although all selected CHRCPs experienced flexural failure, the maximum shear-span-to-depth ratio in the tests was limited to 6.1 due to experimental constraints. The ES values of bridge piers with significantly larger shear-span-to-depth ratios (such as tall-pier bridges) may exhibit some differences. All specimens were tested under idealized fixed-base conditions at the pier bottom. If the soil–foundation interaction is pronounced in actual bridges, the ES of piers may exhibit substantial variations. Furthermore, the test specimens did not account for factors such as the effects of concrete deterioration, steel corrosion, or construction quality on ES. Therefore, when applying the ES model proposed in this study to the aforementioned conditions, further appropriate modifications to the ES are necessary. However, such adjustments fall beyond the scope of this study.

The envelope of the measured lateral load–displacement relationship was corrected for P-delta effects to obtain the effective lateral force–displacement envelope for each pier. Then, the measured effective stiffness ratio ($EI_{\mathrm{eff}}/E_{\mathrm{c}}I_{\mathrm{g}}$) was calculated using the method proposed by Park (1989). The maximum, minimum, mean, median, and coefficient of variation properties of the main design parameters and measured effective stiffness ratio of 52 CHRCPs are reported in Table 2. Table 2 shows that the measured ES ranges from 10% to 50% of the gross-section stiffness $E_{\mathrm{c}}I_{\mathrm{g}}$, and the average value of measured effective stiffness ratio is 0.21.

Table 3 presents the statistical results for the ratio of calculated-to-measured effective stiffness of 50 CHRCP specimens. Most of the existing ES models tend to overestimate the measured ES of CHRCPs; the calculated stiffness is 1.41–2.94 times that of the measured stiffness, and only the stiffness calculated by Wei is less, at 0.9 times that of the measured stiffness. Of these existing procedures, Haselton and Zheng provide the minimum overestimation of the measured ES, but still approximately 40% higher; bridge seismic codes (JTG/T2 231-01-2020, 2008; Caltrans, 2019; Eurocode 8, 2005) significantly overestimate the ES, approximately 1.8 times that of the measured stiffness; the Paulay model is 2.94 times that of the measured stiffness, which is the most severely overestimated.

In addition, the scatter of the results of the existing models is large. According to the test data of 50 CHRCPs, the coefficient of variation for all of these models ranges from 0.25 to 0.41. The coefficient of variation provided by bridge seismic codes is 0.25, and the other models are 0.32–0.41. Considering the maximum, minimum, mean, and coefficient of variation, Zheng and Wei provide relatively good models compared to the existing ES models. Because the mechanical behavior of a rectangular hollow pier is similar to a CHRCP, the average value of ES calculated by the Wei model derived from rectangular hollow piers is the closest to the measured result, but the coefficient of variation is as high as 0.36. To sum up, the existing ES models appropriate for design applications generally tend to overestimate the measured ES of CHRCP and are unacceptably inaccurate. To obtain a more accurate and stable ES model, the main factors affecting the ES of CHRCP must be further studied in detail.

TABLE 1 Existing models of effective stiffness.

Model number	References	Effective stiffness models	Pier type	Structure type	Governing parameters
M1	FEMA 356 (2000)	$EI_{eff}/E_cI_g = 0.5$, $\eta < 0.3$; 0.7, $\eta > 0.5$; $0.3 \leq \eta \leq 0.5$, linear interpolation	Solid	Building	η
M2	ASCE 41-06 (2007)	$EI_{eff}/E_cI_g = 0.3$, $\eta < 0.1$; 0.7, $\eta > 0.5$; $0.1 \leq \eta \leq 0.5$, linear interpolation	Solid	Building	η
M3	Paulay and Priestley (1992)	$EI_{eff}/E_cI_g = 0.4$, $\eta < -0.05$; 0.8, $\eta > 0.5$; $-0.05 \leq \eta \leq 0.5$, linear interpolation	Solid	Building	η
M4	Kumar and Singh (2010)	$EI_{eff}/E_cI_g = 0.175 + 0.875\eta$; and $0.35 \leq EI_{eff}/E_cI_g \leq 0.7$	Rectangular solid	Building	η
M5	Haselton et al. (2008)	$EI_{eff}/E_cI_g = -0.07 + 0.59\eta + 0.07\gamma$; and $0.2 \leq EI_{eff}/E_cI_g \leq 0.6$	Rectangular solid	Building; Bridge	η; γ
M6	Elwood and Eberhard (2009)	$EI_{eff}/E_cI_g = (0.45 + 2.5\eta)/[1 + 110\,(d_b/H)/\gamma]$; and $0.2 \leq EI_{eff}/E_cI_g \leq 1.0$	Solid	Building; Bridge	η; γ; d_b; H
M7	Berry et al. (2008)	$EI_{eff}/E_cI_g = 0.15 + 1.0\eta + 0.035\gamma + 0.10\rho_l \leq 1.0$	Circular solid	Bridge	η; γ; ρ_l
M8	Zheng and Li (2013)	$EI_{eff}/E_cI_g = 0.072 + 0.485\eta + 3.041\rho_l + 0.029\gamma - 0.064 f_y d_b/L\sqrt{f_c'} \leq 1.0$	Solid	Bridge	η; γ; ρ_l; $f_y d_b/L\sqrt{f_c'}$
M9	Wei et al. (2019)	$EI_{eff}/E_cI_g = 0.467\eta + 0.04\gamma - 0.1 f_y d_b/L\sqrt{f_c'}$	Rectangular hollow	Bridge	η; γ; $f_y d_b/L\sqrt{f_c'}$
M10	JTG/T2 231-01-2020 (2008), Caltrans (2019), Eurocode 8 (2005)	$EI_{eff}/E_cI_g = (M_y/\phi_y)/E_cI_g$	Arbitrary shape	Bridge	—

Note: In the table, η is the axial load ratio, γ is the shear-span ratio, ρ_l is the longitudinal reinforcement ratio, d_b is the longitudinal reinforcement diameter, H is the depth of the section, f_y is the yield strength of longitudinal reinforcement, f_c' is the compressive strength of concrete, L is the equivalent height of pier, and the meanings of other symbols are the same as before.

5 Main factors influencing the ES of CHRCPs

Several researchers (Kumar and Singh, 2010; Elwood and Eberhard, 2009; Zheng and Li, 2013) have proposed estimating the yield displacement Δ_y of an equivalent cantilever column of length L as the sum of the flexural deformation, shear deformation, and slip deformation (Equations 4–7).

$$\Delta_y = \Delta_{flex} + \Delta_{shear} + \Delta_{slip} \tag{4}$$

$$\Delta_{flex} = \frac{L^2}{3}\phi_y = \frac{M_y L^2}{3EI_{eff-flex}} \tag{5}$$

$$\Delta_{shear} = \frac{M_y}{k_v A_g G_{eff}} \tag{6}$$

$$\Delta_{slip} = \frac{d_b f_y \phi_y}{8u_b} L \tag{7}$$

where k_v is the shape coefficient, G_{eff} is the effective shear modulus, u_b is the average bond stress between the reinforcement and the footing concrete, and the meanings of other symbols are the same as before.

Therefore, the main factors influencing the effective stiffness (ES) of CHRCPs can be identified based on the theoretical framework of the simplified three-component model for yield displacement. For flexural deformation, because the factors that affect the effective flexural stiffness also affect the ES, the influencing factors of flexural effect on the ES of CHRCPs can be identified by studying the influencing factors of effective flexural stiffness. For shear and slip deformations, the calculation of yield displacement using Equation 2 assumes that both shear and slip

TABLE 2 Key parameters and statistics of circular hollow piers.

No.	Pier name	L (mm)	D (mm)	d (mm)	L/D	α_g	ρ_l (%)	$P/A_g f_c'$	f_c' (MPa)	f_y (MPa)	d_b (mm)	$EI_{eff}/E_c I_g$
Whittaker et al. (1987)												
1	DU5	3,200	800	700	4.0	0.77	2.88	0.30	37.0	430	6	0.50
2	DU6	3,200	800	700	4.0	0.77	2.88	0.30	33.0	430	6	0.49
Zahn et al. (1990)												
3	FU1	1,625	400	212	4.1	0.28	3.56	0.08	29.6	306	16	0.37
4	FU3	1,625	400	250	4.1	0.39	4.20	0.10	29.6	306	16	0.38
5	FU5	1,625	400	290	4.1	0.53	5.40	0.12	27.3	306	16	0.48
Unjoh and ASAZU (1999)												
6	F1	3,000	750	450	4.0	0.36	4.27	0.08	25.9	382	16	0.38
7	F2	3,000	750	450	4.0	0.36	4.27	0.07	28.0	382	16	0.35
8	F3	3,000	750	450	4.0	0.36	4.27	0.06	32.3	382	16	0.33
Chung et al. (1999)												
9	CH1P1L1	2032	600	332	3.4	0.31	1.16	0.09	24.2	420	9.5	0.17
10	CH1P1L2	2032	600	332	3.4	0.31	1.16	0.09	24.2	420	9.5	0.16
11	CH1P2L1	2032	600	332	3.4	0.31	1.16	0.15	24.2	420	9.5	0.15
12	CH2P1L1	2032	600	332	3.4	0.31	1.16	0.09	24.2	420	9.5	0.17
13	CH2P1L2	2032	600	332	3.4	0.31	1.16	0.09	24.2	420	9.5	0.20
Hoshikuma and Priestley (2000)												
14	HF1	6,528	1,524	1,245	4.3	0.67	1.49	0.13	37.4	427	13	0.33
Ranzo and Priestley (2001)												
15	HS1	3,880	1,560	1,256	2.5	0.65	1.34	0.05	40.0	450	13	0.12

(Continued on the following page)

10.3389/fbuil.2025.1629114

TABLE 2 (*Continued*) Key parameters and statistics of circular hollow piers.

No.	Pier name	L (mm)	D (mm)	d (mm)	L/D	α_g	ρ_l (%)	$P/A_g f_c'$	f_c' (MPa)	f_y (MPa)	d_b (mm)	$EI_{eff}/E_c I_g$
Zhu et al. (2009)												
16	Z1	3,070	500	400	6.1	0.64	1.67	0.09	28.9	462	10	0.30
17	Z2	3,070	500	300	6.1	0.36	1.00	0.09	31.9	462	10	0.32
18	Z4	3,070	500	360	6.1	0.52	1.66	0.15	34.9	462	10	0.26
Kim and Kang (2012)												
19	HC-IO-90-L	2,800	800	400	3.5	0.25	1.07	0.10	22.4	442	16	0.16
20	HC-IO-90-H	2,800	800	400	3.5	0.25	1.07	0.10	22.4	442	16	0.16
Kim et al. (2014)												
21	C-L	4,900	1,400	980	3.5	0.49	1.30	0.10	22.0	376	19	0.14
22	C-T	4,900	1,400	980	3.5	0.49	1.30	0.10	22.0	376	19	0.16
23	C-NT	4,900	1,400	980	3.5	0.49	1.30	0.10	22.0	376	19	0.15
Kim et al. (2016)												
24	S-CHC-80	4,900	1,400	1,050	3.5	0.56	1.52	0.10	28.1	408	19	0.17
25	S-CHT-80	4,900	1,400	1,050	3.5	0.56	1.52	0.10	24.3	408	19	0.17
26	S-CHNT-80	4,900	1,400	1,050	3.5	0.56	1.52	0.10	27.4	408	19	0.16
Lee et al. (2015)												
27	P2	3,500	1,000	500	3.5	0.25	1.16	0.09	32.5	499	19	0.20
28	P3	3,500	1,000	500	3.5	0.25	1.35	0.09	32.5	499	19	0.19
29	P4	3,500	1,000	500	3.5	0.25	1.16	0.09	32.5	499	19	0.21
30	P5	3,500	1,000	750	3.5	0.56	1.98	0.15	32.5	499	19	0.26
31	P6	3,500	1,000	500	3.5	0.25	1.35	0.09	32.5	499	19	0.20
32	P7	3,500	1,000	500	3.5	0.25	1.35	0.09	32.5	499	19	0.19
33	P8	3,500	1,000	750	3.5	0.56	1.16	0.09	32.5	499	19	0.17

(Continued on the following page)

10.3389/fbuil.2025.1629114

TABLE 2 (*Continued*) Key parameters and statistics of circular hollow piers.

No.	Pier name	L (mm)	D (mm)	d (mm)	L/D	α_g	ρ_l (%)	$P/A_g f_c'$	f_c' (MPa)	f_y (MPa)	d_b (mm)	$EI_{eff}/E_c I_g$
34	RP1	4,900	1,400	980	3.5	0.49	1.01	0.09	39.0	481	19	0.11
35	RP2	4,900	1,400	980	3.5	0.49	1.01	0.09	39.0	481	19	0.12
36	RP3	4,900	1,400	980	3.5	0.49	1.01	0.09	39.0	481	19	0.11
37	RP4	4,900	1,400	980	3.5	0.49	1.01	0.09	39.0	481	19	0.11
38	RP5	4,900	1,400	980	3.5	0.49	1.01	0.09	39.0	481	19	0.10
39	RP6	4,900	1,400	980	3.5	0.49	1.01	0.09	39.0	481	19	0.10
40	RP7	4,900	1,400	980	3.5	0.49	1.01	0.09	39.0	481	19	0.10
41	RP8	4,900	1,400	980	3.5	0.49	1.01	0.09	39.0	481	19	0.10
42	RP9	4,900	1,400	980	3.5	0.49	2.02	0.09	39.0	481	19	0.12
43	RP10	4,900	1,400	980	3.5	0.49	2.02	0.09	39.0	481	19	0.12
44	RP11	4,900	1,400	980	3.5	0.49	1.01	0.13	27.5	481	19	0.14
45	RP12	4,900	1,400	980	3.5	0.49	1.01	0.13	27.5	481	19	0.13
46	RP13	4,900	1,400	980	3.5	0.49	1.01	0.13	27.5	481	19	0.14
Liang et al. (2021a)												
47	S1	3,850	1,000	800	3.9	0.64	1.62	0.18	32.1	457	18	0.30
48	S2	3,850	1,000	750	3.9	0.56	1.33	0.15	32.5	457	18	0.24

(Continued on the following page)

10.3389/fbuil.2025.1629114

TABLE 2 (*Continued*) Key parameters and statistics of circular hollow piers.

No.	Pier name	L(mm)	D(mm)	d(mm)	L/D	α_g	ρ_l(%)	$P/A_g f_c'$	f_c'(MPa)	f_y(MPa)	d_b(mm)	$EI_{eff}/E_c I_g$
Li et al. (2020), Liang et al. (2021b)												
49	S3	3,850	1,000	600	3.9	0.36	1.82	0.09	33.8	457	18	0.20
50	S4	3,850	1,000	600	3.9	0.36	1.82	0.10	31.6	457	18	0.25
A total of 50 piers	Maximum	6,528	1,560	1,256	6.1	0.77	5.4	0.30	40.0	499	19	0.50
	Minimum	1,625	400	212	2.5	0.25	1.0	0.05	22.0	306	6	0.10
	Median	3,675	1,000	725	3.50	0.49	1.3	0.09	32.2	457	19	0.17
	Mean	3,773	1,037	702	3.8	0.45	1.7	0.11	31.1	442	16	0.21
	Coefficient of variation	0.31	0.35	0.43	0.18	0.31	0.62	0.43	0.19	0.12	0.25	0.51
Yeh et al. (2001)												
51	PS1-C	5,500	1,500	900	3.7	0.36	2.2	0.10	31.7	418	22	0.22
Kim and Kang (2012)												
52	HCO-100	2,800	800	400	3.5	0.25	1.1	0.10	22.4	442	16	0.18

Note: In the table, d is the inner diameter, α_g is the hollow ratio, and the meanings of other symbols are the same as before.

10.3389/fbuil.2025.1629114

10.3389/fbuil.2025.1629114

deformations are transformed into equivalent flexural deformation. Therefore, the influencing factors of shear effect and slip effect on the ES of CHRCPs can be identified by studying the relative relationship between shear deformation, slip deformation, and flexural deformation.

5.1 Factors influencing flexural deformation

To investigate the factors that influence flexural deformation (or effective flexural stiffness), taking the full-scale CHRCPs in China as the prototype (Yeh et al., 2001), a parameter analysis was carried out to consider the axial load ratio and longitudinal reinforcement ratio for a typical bridge pier. The following basic data were assumed: (1) pier outer diameter:1.5 m; (2) pier inner diameter:0.9 m; (3) cover to longitudinal reinforcement:4 cm; (4) transverse reinforcement diameter and spacing: 13 mm, 100 mm; (5) concrete compressive strength: $f_c' = 32$ MPa; (6) yield strength of longitudinal reinforcement: $f_y = 420$ MPa; (7) axial load ratio: $P/A_g f_c' = 0$ to 0.35 (8 levels); (8) longitudinal reinforcement ratio: $\rho_l = 0.5\%–4.0\%$ (5 levels).

Based on the computed moment–curvature relationship, the effective flexural stiffness of the pier $EI_{\text{eff-flex}}$ can be determined using the idealized yield moment M_y and idealized yield curvature ϕ_y, as shown in Figure 1. Therefore, the factors influencing effective flexural stiffness can be identified through the parameter analysis of M_y and ϕ_y. The moment–curvature curve was determined based on plane-section analysis using the concrete constitutive model by Mander et al. (1988) and a linear constitutive model for steel. The section division of CHRCP is shown in Figure 3. For the parametric study, eight levels of axial load ratio were considered for each longitudinal reinforcement ratio, resulting in a total of 40 analysis cases. To facilitate comparison and interpretation, the dimensionless equivalent yield moment M_{Dy} and dimensionless equivalent yield curvature ϕ_{Dy} are respectively defined as follows (Equations 8, 9):

$$M_{Dy} = \frac{M_y}{f_c' D^3} \tag{8}$$

$$\phi_{Dy} = \frac{\phi_y D}{\varepsilon_y} \tag{9}$$

where ε_y is the yield strain of longitudinal reinforcement, and the meanings of other symbols are the same as before.

As shown in Figure 4a, the equivalent yield moment is significantly influenced by both the axial load ratio and the longitudinal reinforcement ratio, exhibiting a clear increasing trend with the rise of either parameter. In contrast, it is observed that the dimensionless equivalent yield curvature is comparatively insensitive to variations in the axial load ratio and longitudinal reinforcement ratio. Figure 4b shows the average value of dimensionless equivalent yield curvature ($\phi_{Dy} = 2.18$), along with reference lines representing ±15% of this mean. It is seen that most data, except those for low reinforcement ratios coupled with very high axial load ratios, fall within the ±15% limits. This suggests that the equivalent yield curvature remains essentially stable across a wide range of design parameters and is not affected by the flexural capacity of the section.

TABLE 3 Statistics for the ratios of calculated-to-measured effective stiffness values for existing ES models.

Statistics	FEMA356 M1	ASCE 41 M2	Paulay M3	Kumar M4	Haselton M5	Elwood M6	Berry M7	Zheng M8	Wei M9	JTG, Caltrans Eurcode8 M10
Maximum	4.88	2.93	4.88	3.42	2.21	4.58	3.53	2.22	1.48	2.80
Minimum	0.99	0.67	1.09	0.73	0.59	0.75	0.87	0.78	0.34	0.87
Median	2.92	1.75	2.93	2.05	1.38	2.59	2.10	1.34	0.83	1.77
Mean	2.88	1.78	2.94	2.03	1.41	2.75	2.18	1.42	0.90	1.82
Coefficient of variation	0.41	0.38	0.39	0.40	0.33	0.40	0.36	0.32	0.36	0.25

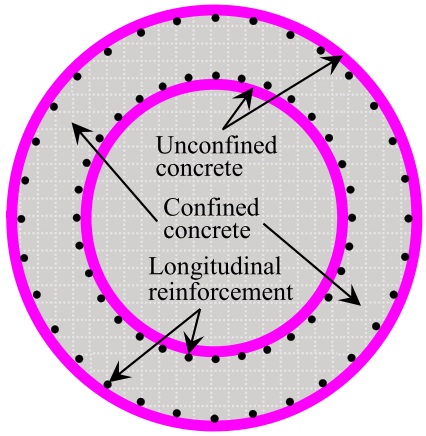

FIGURE 3
Section division of CHRCP.

It should be noted that although the data were generated from specific CHRCP sizes and material strengths, the dimensionless results are expected to be broadly applicable to other CHRCP configurations and material strengths within the typical range used in standard design practice (Priestley et al., 2007).

Combined with the data in Figure 4 and Equation 1, the axial load ratio and longitudinal reinforcement ratio can be identified as the governing parameters for the effective flexural stiffness of CHRCPs. To directly quantify their influence, the ratio of effective flexural stiffness to gross-section stiffness β_g is defined by Equation 10.

$$\beta_g = \frac{EI_{\text{eff-flex}}}{E_c I_g} \tag{10}$$

where E_c is the concrete modulus of elasticity (E_c can be taken as $5000\sqrt{f'_c}$MPa (Priestley et al., 2007)), and I_g is the gross-section moment of inertia. The results are shown in Figure 5 for the ranges of axial load ratio and longitudinal reinforcement ratio considered. It will be seen that the effective flexural stiffness ratio varies between 0.09 and 0.84. The data shown in Figure 5 can be used to determine the effective flexural stiffness of the piers as a function of axial load ratio and longitudinal reinforcement ratio. Therefore, the ES (EI_{eff}) of CHRCPs will increase with the increase in axial load ratio ($P/A_g f_c^{'}$) and longitudinal reinforcement ratio (ρ_l).

Note that Figure 5 shows that as the longitudinal reinforcement ratio increases, its influence on the effective flexural stiffness tends to weaken with higher axial compression ratios, indicating a certain interactive effect between the longitudinal reinforcement ratio and the axial compression ratio on the effective flexural stiffness. This interaction largely depends on how the longitudinal reinforcement ratio and axial compression ratio affect the idealized yield curvature, which can be intuitively observed from the consistent trends between Figures 4b, 5.

5.2 Factors influencing shear deformation

Compared with solid piers, the shear capacity of hollow piers is significantly reduced due to the presence of a hollow section, making the contribution of shear deformation to the equivalent yield displacement more pronounced (Sun et al., 2013). As the degree of hollowness increases, the shear capacity decreases accordingly. Thus, the effect of hollowness on the ES of the CHRCP should be considered. To describe the hollowness of hollow section, a dimensionless parameter α_g (hollow ratio) is introduced, which is defined as the ratio of the area of hollow part to the cross-sectional area of the hollow pier as if it were solid. For the CHRCP, α_g is given by Equation 11.

$$\alpha_g = (d/D)^2 \tag{11}$$

where d is the inner diameter, and D is the outer diameter.

For the cantilever CHRCP, after introducing the dimensionless parameters α_g and β_g, Equation 5, used to calculate the flexural deformation of the yield displacement, can be rewritten as Equation 12.

$$\Delta_{\text{flex}} = \frac{64 M_y L^2}{3\beta_g \pi D^4 \left(1-\alpha_g^2\right) E_c} \tag{12}$$

Equation 6 used to calculate the shear deformation of the yield displacement can be rewritten as Equation 13.

$$\Delta_{\text{shear}} = \frac{4M_y}{k_v \pi D^2 \left(1-\alpha_g\right) G_{\text{eff}}} \tag{13}$$

For a circular section, the shape coefficient (k_v) can be taken as 0.85 (Elwood and Eberhard). The concrete effective shear modulus (G_{eff}) depends on the modulus of elasticity of concrete and Poisson's ratio of concrete (υ); that is, $G_{\text{eff}} = E_c/[2\ (1+\upsilon)]$. For normal-weight concrete, the value of Poisson's ratio can be taken as 0.2. Based on these assumptions, the ratio of shear deformation to flexural deformation can be simplified as

$$\frac{\Delta_{\text{shear}}}{\Delta_{\text{flex}}} = \frac{0.53\beta_g}{\left[1/\sqrt{1+\alpha_g} \times (L/D)\right]^2} \tag{14}$$

The parameter $(1/\sqrt{1+\alpha_g})$ before the shear-span ratio (L/D) in Equation 14 is defined as the equivalent shear-span ratio coefficient, which can be regarded as the reduction coefficient of the shear-span ratio when calculating the ratio of shear deformation to flexural deformation. The hollow ratio is between 0 and 1; thus, the equivalent shear-span ratio coefficient is between 0.71 and 1.00; that is, the effect of reducing the hollow ratio on the shear-span ratio is limited. Figure 6 shows the relationship between hollow ratio and equivalent shear-span ratio coefficient. The analyzed CHRCP specimens exhibited hollow ratios of 0.25–0.77 (mean = 0.45) and equivalent shear-span ratio coefficients of 0.75–0.89 (mean = 0.83).

From Equation 14 and Figure 6, it can be seen that the contribution of shear deformation to equivalent yield displacement decreases with the increase in shear-span ratio (L/D), and increases with the increase in hollow ratio (α_g). Therefore, the ES of the CHRCP increases with the increase in the shear-span ratio and decreases with the increase in the hollow ratio. The coupling effect of shear-span ratio and hollow ratio can be reflected through the equivalent shear-span ratio $1/\sqrt{1+\alpha_g}(L/D)$, and the ES (EI_{eff}) increases with the increase in the equivalent shear-span ratio.

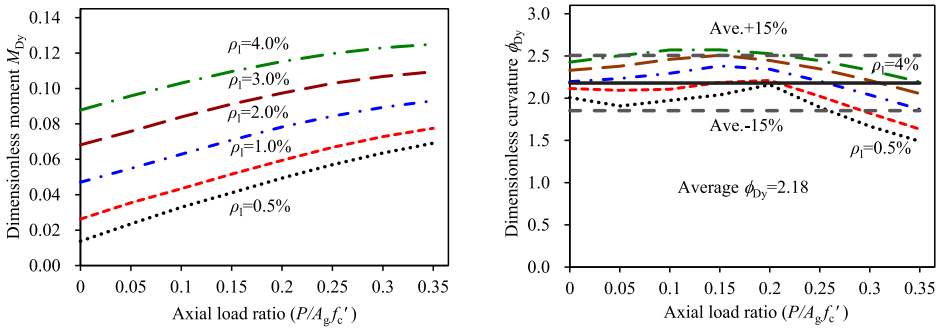

(a) Equivalent yield moment (b) Equivalent yield curvature

FIGURE 4
(a) Equivalent yield moment and **(b)** Equivalent yield curvature. Dimensionless equivalent yield moment and curvature of CHRCPs.

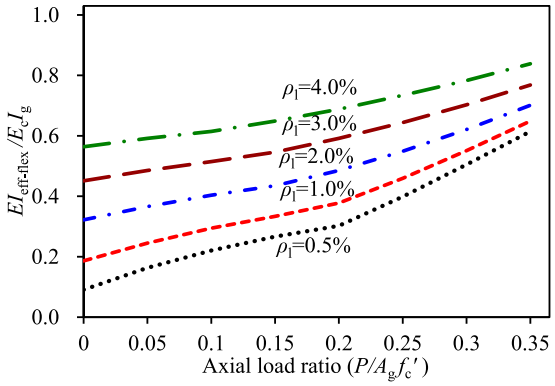

FIGURE 5
Effective flexural stiffness ratio for CHRCPs.

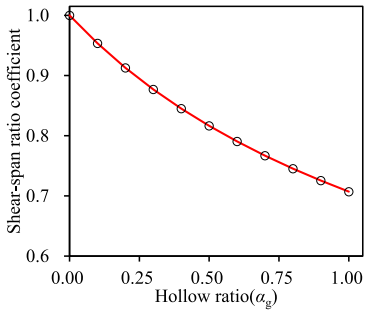

FIGURE 6
Variation of equivalent shear-span ratio coefficients with hollow ratio.

5.3 Factors influencing slip deformation

For the purpose of this study, a uniform bond stress of u_b = $1.0\sqrt{f_c'}$MPa is assumed in the elastic range (Sezen and Setzler, 2008). Based on Equations 5,7, the ratio of slip deformation to flexural deformation can be expressed as

$$\frac{\Delta_{slip}}{\Delta_{flex}} = \frac{3}{8} \times \frac{d_b f_y}{L\sqrt{f_c'}} \tag{15}$$

It can be seen from Equation 15 that the contribution of slip deformation to equivalent yield displacement increases with the increase of parameter $f_y d_b/L\sqrt{f_c'}$. Therefore, the ES (EI_{eff}) of the CHRCP decreases with the increase of $f_y d_b/L\sqrt{f_c'}$.

5.4 Experimental verification of main influencing factors of ES

According to the aforementioned parametric study based on the three-component yield displacement model, the main factors influencing the ES of CHRCP are the axial load ratio ($P/A_g f_c'$), the longitudinal reinforcement ratio (ρ_l), the equivalent shear-span ratio $1/\sqrt{1+\alpha_g(L/D)}$, and $f_y d_b/L\sqrt{f_c'}$. Furthermore, the ES increases with the increase of all influencing factors except $f_y d_b/L\sqrt{f_c'}$. To verify the theoretical results, Figure 7 shows the influencing trend and correlation coefficient of main factors on the measured ES ratio (EI_{eff}/E_cI_g) of 50 CHRCPs. It can be seen from Figure 7 that the variation trend of measured ES with the axial load ratio, longitudinal reinforcement ratio, and equivalent shear-span ratio is consistent with the theoretical analysis.

The research on solid piers by Zheng and Li (2013) shows that the correlation coefficient between the parameter $f_y d_b/L\sqrt{f_c'}$ and the measured ES ratio is −0.54, indicating that the experimental results are consistent with the theoretical analysis. However, for the CHRCPs in this work, the correlation coefficient between the parameter $f_y d_b/L\sqrt{f_c'}$ and the measured ES ratio is only 0.02, as shown in Figure 7, indicating that their correlation is extremely weak and inconsistent with the theoretical results.

The possible reasons are as follows: first, the calculation model of slip deformation is derived from a solid pier with a single layer longitudinal reinforcement, which is not necessarily

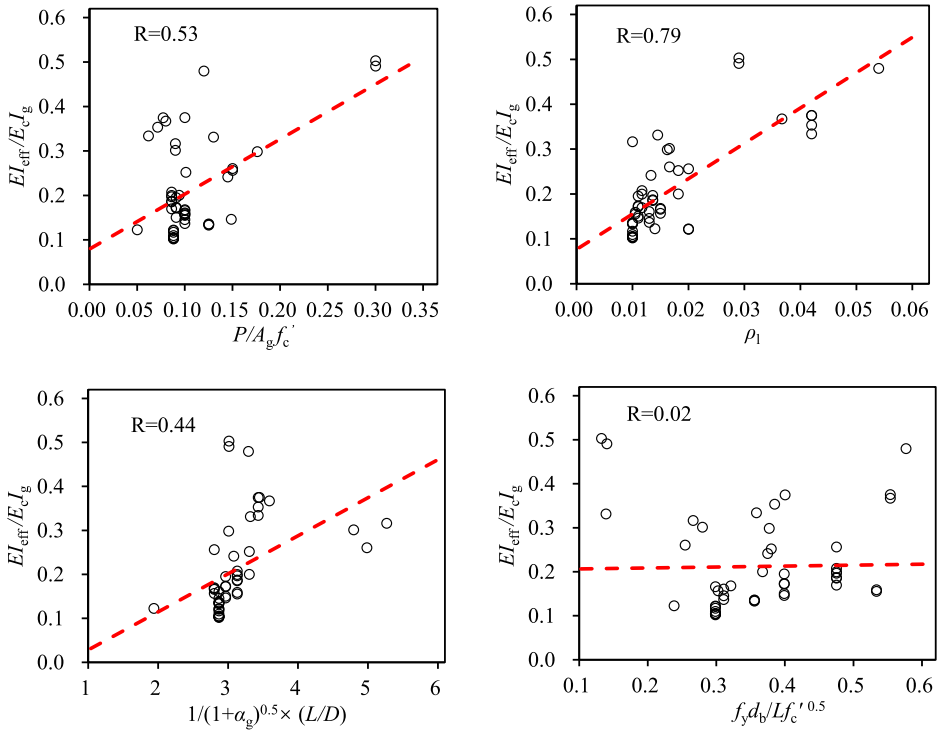

FIGURE 7
Effect of key parameters on measured ES of CHRCPs.

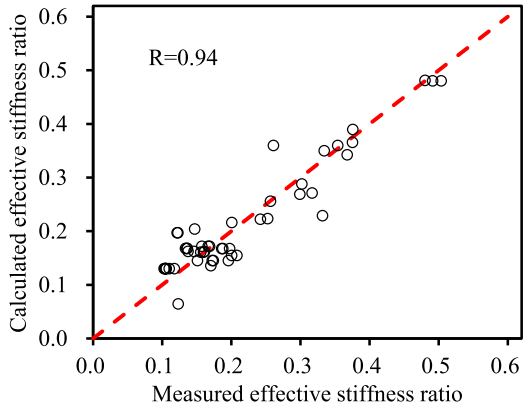

FIGURE 8
Comparison of calculated (Equation 17) and measured ES values.

suitable for a hollow pier with inner and outer longitudinal reinforcement; second, the cross-section is discontinuous due to the hollowness; thus, the assumption that the bottom section of pier rotates around its neutral axis is not completely consistent with the actual situation when the longitudinal reinforcement slipping. Thus, the impact of hollowness on slip deformation remains unclear, requiring further theoretical and experimental investigation (Wang et al., 2019).

6 Calibration and evaluation of the ES model for CHRCPs

6.1 Calibration of the ES model

Based on the theoretical analysis and experimental validation of the main factors influencing the ES conducted in this study, as well as a comprehensive review of the governing parameters considered in existing models, a new four-parameter calibration model for the ES of CHRCPs is proposed.

$$\frac{EI_{\text{eff}}}{E_cI_g}=\lambda_1+\lambda_2\frac{P}{A_gf_c'}+\lambda_3\rho_l+\lambda_4\frac{1}{\sqrt{1+\alpha_g}}\frac{L}{D}\le 1.0 \tag{16}$$

where λ_1~λ_4 are the parameters to be calibrated. Because the axial load ratio, longitudinal reinforcement ratio, hollow ratio, and shear-span ratio of hollow pier are relatively easy to determine, Equation 16 is suitable as the calculation model of ES of CHRCP.

Based on the measured ES ratio EI_{eff}/E_cI_g, axial load ratio P/A_gf_c', longitudinal reinforcement ratio ρ_l, and equivalent shear-span ratio $1/\sqrt{1+\alpha_g}(L/D)$ of 50 CHRCPs collected in this manuscript, the parameters λ_1~λ_4 are calibrated using multiple linear regression in SPSS version 25 software package, and the calibration results are as follows:

$$\frac{EI_{\text{eff}}}{E_cI_g}=-0.192+1.014\frac{P}{A_gf_c'}+6.680\rho_l+0.058\frac{1}{\sqrt{1+\alpha_g}}\frac{L}{D}\le 1.0 \tag{17}$$

TABLE 4 Statistics for ratio of calculated to the measured ES.

Statistics	Zheng M7 (Zheng and Li, 2013)	Wei M8 (Wei et al., 2019)	Proposed Equation 17
Max	2.22	1.48	1.62
Min	0.78	0.34	0.53
Med	1.34	0.83	1.01
Mean	1.42	0.90	1.04
CV	0.32	0.36	0.21
RMSE	0.08	0.10	0.04
MAPE	47.3%	29.6%	16.7%
R^2	0.82	0.34	0.88

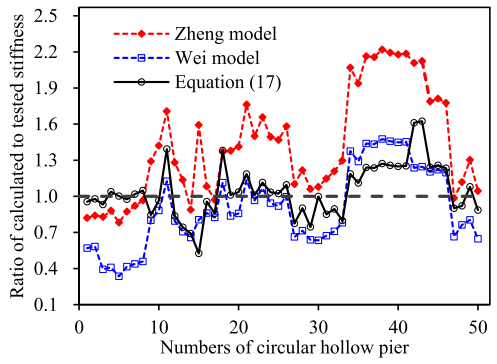

FIGURE 9
Comparison of the ratios of calculated-to-measured ES values.

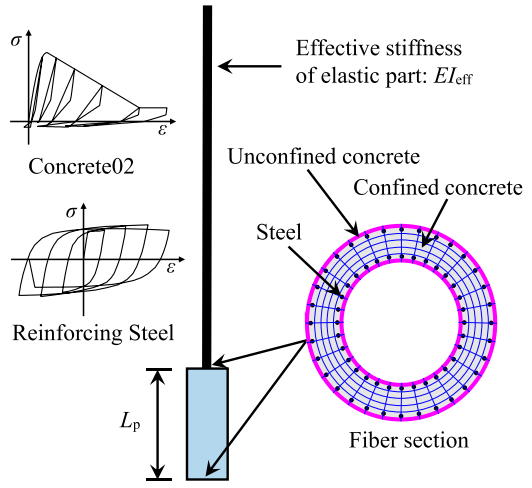

FIGURE 10
Fiber model of Beam with Hinges element.

Because the regression coefficients in Equation 17 were determined using ordinary least squares (OLS) linear regression, the independent variables were not normalized or standardized prior to regression. Figure 8 shows the comparison between the ES ratio of CHRCP calculated by Equation 17 and the measured values. It can be seen from Figure 8 that the calculated results are in good agreement with the experimental results, and the linear correlation coefficient is 0.94. Therefore, within the range of design parameters picked up in this work, Equation 17 gives an accurate estimate of ES of CHRCPs.

It should be noted that the linear model was adopted for the ES model in this study due to its advantages of concise form and convenience for engineering applications. Although Equation 17 incorporates the coupling effect of shear-span ratio and void ratio through the equivalent shear-span ratio, the linear model does not account for potential interactions or nonlinearities between parameters such as axial compression ratio and longitudinal reinforcement ratio. This may somewhat compromise the accuracy of the ES estimation. To address this limitation, future research should collect more experimental data and employ methods such as machine learning algorithms or nonlinear regression. This would enable a more profound insight into the potential interaction effects and nonlinear influences among parameters, facilitating the development of a more precise predictive model for ES.

6.2 Evaluation of ES models

To compare the proposed model with the Zheng model (Zheng and Li, 2013) and the Wei model (Wei et al., 2019), which give relatively accurate results in the existing ES models, Table 4 presents statistical parameters comparing the calculated-to-experimental ES values of 50 CHRCPs using Zheng's formula, Wei's formula, and the proposed formula. The evaluated metrics include maximum (Max), minimum (Min), median (Med), mean (Mean), coefficient of variation (CV), root mean square error (RMSE), mean absolute percentage error (MAPE), and coefficient of determination (R^2). Figure 9 shows the ratio of calculated-to-measured ES for each pier. It can be observed from Table 4 and Figure 9 that: (1) The

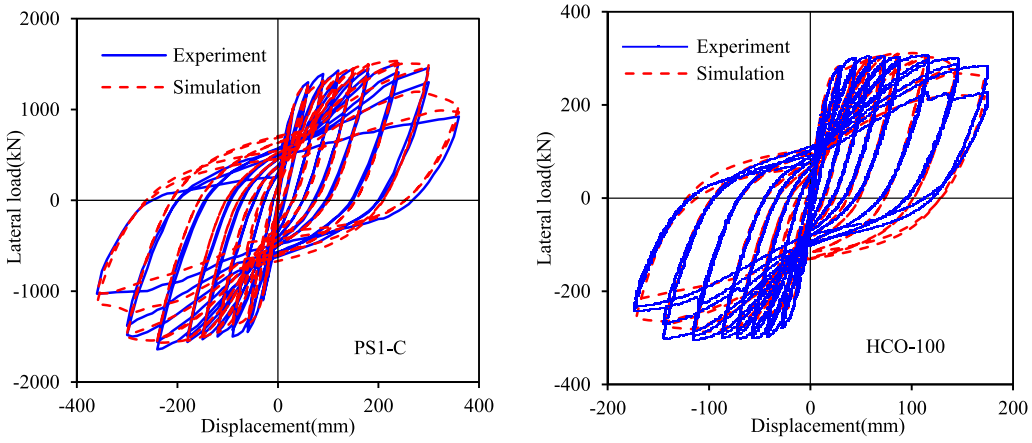

FIGURE 11
Comparisons for hysteretic curves of CHRCPs.

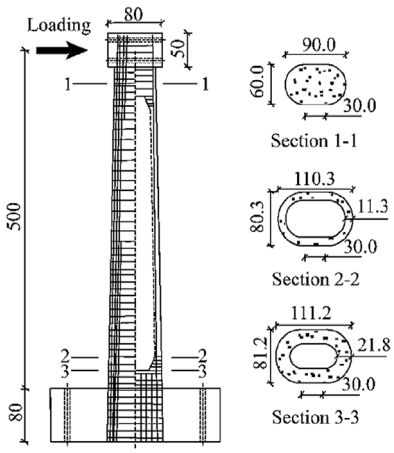

FIGURE 12
Size and rebar arrangement of specimen (unit: cm) (Shao et al., 2019).

ES of CHRCPs calculated by the proposed formula Equation 17 demonstrates the closest agreement with the experimental results. The corresponding mean value and coefficient of variation are 1.04 and 0.21, respectively. Moreover, the proposed formula achieves the smallest RMSE (0.04) and MAPE (16.7%), along with the highest R^2 (0.88), indicating superior error statistics and significantly enhanced prediction accuracy compared to the other two. For CHRCP, the calculated mean of the Wei model is close to the experimental value, which is 0.90, but the coefficient of variation is as high as 0.36; the results of the Zheng model are relatively poor in terms of mean and coefficient of variation, which are 1.40 and 0.32, respectively. (3) The fluctuation trends of the ratio of calculated to the measured ES given by the Zheng model, the Wei model, and Equation 17 are basically the same, and the fluctuation amplitudes (the difference between the maximum and minimum value) are 1.44, 1.14, and 1.09, respectively. Furthermore, most of the calculation results of Equation 17 fall between the results of the Zheng model and the Wei model. (4) It is noteworthy that, although discrepancies exist in prediction accuracy among the Zheng, Wei, and proposed models, all three models exhibit consistent increasing and decreasing trends across the 50 circular hollow pier specimens (as shown in Figure 9). This coherence demonstrates that these models collectively capture the sensitivity of ES to dominant parameters (axial compression ratio, longitudinal reinforcement ratio, shear-span ratio, etc.), reflecting the fundamental mechanical principles governing circular hollow piers. Moreover, this consistency implicitly validates the reliability of both the experimental dataset and data processing methodology.

Therefore, compared with the existing models, the model proposed in this work is more reasonable and stable for estimation of the ES of CHRCPs. In addition, the ES model proposed in this work is easy to apply and only requires determination of the axial load ratio, the longitudinal reinforcement ratio, the hollow ratio, and the shear-span ratio. It does not require determination of the longitudinal reinforcement diameter and yield strength, etc., and does not require complex moment–curvature analysis.

7 Verification of ES model for CHRCPs

7.1 Simulation of force–displacement response for CHRCPs

To further illustrate the validity of Equation 17, except for the 50 CHRCPs used for model calibration, another two piers (full-scaled pier PS1-C (Yeh et al., 2001) and scaled pier HCO-100 (Kim and Kang, 2012)) are used to verify the validity of Equation 17 on the simulation of lateral force–displacement response. The main design parameters of piers PS1-C and HCO-100 are shown in Table 2.

The overall force–displacement hysteretic curves for both piers were simulated based on a static reversed-cyclic analysis using OpenSees. In this manuscript, the piers are modeled as a Beam with Hinges element (OpenSees, 2024) proposed by Scott and Fenves (2006). The model assumes that the inelastic deformation is concentrated in the length L_p of the plastic hinge at the bottom of the pier, while the upper part of the plastic hinge remains elastic. When

TABLE 5 Statistics of key parameters for round-end piers.

No.	L/H	α_g	ρ_l (%)	ρ_s (%)	$P/A_g f_c'$	f_c' (MPa)	f_y (MPa)	L (mm)	d_b (mm)
Shao et al. (2019)									
SA1	6.2	0.62	0.91	0.33	0.15	32.0	459	5,000	12
SA2	6.2	0.62	0.91	0.91	0.15	34.7	459	5,000	12
SA3	6.2	0.62	0.91	1.51	0.15	32.0	459	5,000	12
SB1	6.2	0.62	0.91	0.91	0.11	32.0	459	5,000	12
SB2	6.2	0.62	0.91	0.91	0.14	33.4	459	5,000	12
Jiang et al. (2024)									
HOL1	2.6	0.56	0.80	0.50	0.15	38.8	405	3,000	10
HOL6	3.3	0.58	0.50	0.15	0.15	40.2	452	4,000	8
HOL8	4.8	0.58	0.20	0.50	0.10	38.8	452	4,000	8
HOL9	4.0	0.60	0.80	0.15	0.10	36.1	405	5,000	10
HOL10	4.0	0.60	0.20	0.30	0.15	41.7	452	5,000	8
HOL11	4.0	0.60	0.50	0.50	0.05	40.4	405	5,000	10

Note: In the table, ρ_s is the volumetric stirrup ratio, and $P/A_g f_c'$ is the measured axial load ratio.

a plastic hinge forms at the pier base (i.e., when the base-section curvature exceeds the idealized yield curvature), the equivalent plastic hinge length L_p remains constant, as illustrated in Figure 10. To match the experimental loading conditions, the bottom node of the Beam with Hinges element was fully fixed, while the top node remained unconstrained to allow application of axial force and lateral displacement (or force). It should be noted that the Beam with Hinges element is particularly suitable for quasi-static pushover analysis of piers exhibiting typical flexural failure modes. The two most critical parameters of this model are the plastic hinge length L_p and the ES EI_{eff}, as shown in Figure 10. In the numerical simulation of fiber element based on the principle of curvature integration, it is more reasonable to use the plastic hinge length that matches the plastic curvature derived from moment–curvature analysis (Li et al., 2016). Therefore, in the static reversed-cyclic analysis, the plastic hinge length L_p is determined by Equation 18 suggested by Li et al. (2016), and the ES is calculated by Equation 17. The calculated values of the ES ratios (EI_{eff}/E_cI_g) of piers PS1-C and HCO-100 are 0.236 and 0.161, respectively, while the corresponding measured values are 0.216 and 0.177, and the relative errors are not larger than 10%.

$$L_p = 5.65\rho_l L + 0.325D + 0.09\frac{f_y d_b}{\sqrt{f_c'}} \quad (18)$$

For each pier, a fiber section composed of unconfined concrete, confined concrete, and steel material was initially established. In this study, the Concrete02 material model in the software of OpenSees was adopted for unconfined concrete and confined concrete, and the Reinforcing Steel uniaxial material model was used to simulate the longitudinal reinforcement. This model considers the mechanical effects of strain softening, low-cycle fatigue, and tensile fracture of the bars (Kunnath et al., 2009). The division of fiber section and the constitutive relationship of uniaxial material are shown in Figure 10.

Figure 11 shows the comparison between the simulated results and the experimental results of the force–displacement hysteresis curves of the full-scale pier PS1-C and scaled pier HCO-100. For full-scale and scaled bridge piers, the calculated results are in good agreement with the experimental results, and the initial stiffness, unloading stiffness, and reloading stiffness under low-cycle loads can be simulated accurately. These results indicate that the ES model proposed in this manuscript is reasonable and reliable to estimate the ES of CHRCPs.

Bridge seismic design codes, such as Caltrans, Eurocode 8, and China's JTG, typically recommend using the effective flexural stiffness as the ES of the bridge pier. For the two representative CHRCP specimens, PS1-C and HC-O-100, the effective flexural stiffness ratio ($EI_{eff\text{-}flex}/E_cI_g$) are 0.383 and 0.278, respectively. These values indicate that the ES values prescribed by the seismic codes are approximately 1.62 and 1.73 times greater than the ES estimated by the model proposed in this work. This overestimation implies that using effective flexural stiffness as a proxy for overall ES can lead to a substantial underestimation of displacement demands under the same level of horizontal seismic loading. In practice, this means the predicted displacements will be smaller than those observed experimentally, which may compromise the reliability of deformation assessments and increase the risk of unseated spans. While a detailed investigation into span unseating risk is beyond the scope of this study, it highlights the critical importance of using a more accurate estimation of pier stiffness in seismic design.

TABLE 6 Comparison of ES ratios for round-end piers.

No.	Measured	Zheng M7			Wei M8			This work Equation 17		
		Predicted	Predicted/measured	RE	Predicted	Predicted/measured	RE	Predicted	Predicted/measured	RE
SA1	0.289	0.339	1.173	17%	0.298	1.032	3%	0.302	1.045	4%
SA2	0.383	0.340	0.887	11%	0.299	0.781	22%	0.302	0.788	21%
SA3	0.357	0.339	0.950	5%	0.298	0.836	16%	0.302	0.846	15%
SB1	0.228	0.320	1.402	40%	0.280	1.227	23%	0.261	1.146	15%
SB2	0.259	0.334	1.291	29%	0.294	1.136	14%	0.292	1.127	13%
HOL1	0.120	0.230	1.916	92%	0.152	1.264	26%	0.134	1.112	11%
HOL6	0.124	0.247	1.986	99%	0.188	1.514	51%	0.146	1.175	18%
HOL8	0.144	0.257	1.783	78%	0.225	1.560	56%	0.145	1.006	1%
HOL9	0.175	0.251	1.438	44%	0.192	1.098	10%	0.145	0.829	17%
HOL10	0.180	0.259	1.434	43%	0.218	1.206	21%	0.155	0.861	14%
HOL11	0.093	0.218	2.348	135%	0.169	1.821	82%	0.074	0.797	20%
Mean	0.214	0.285	1.510	54%	0.238	1.225	29%	0.205	0.976	14%

10.3389/fbuil.2025.1629114

Moreover, the need for accurate ES estimation becomes even more critical in nonlinear time-history analyses, where the displacement response of bridge structures is highly sensitive to the peaks and troughs of the ground motion response spectrum.

7.2 Estimation of ES for round-ended hollow piers

Round-ended hollow piers are widely employed in railway bridges in China. To investigate the seismic performance of such piers, Shao et al. (2019) conducted low-cycle reversed loading tests on five 1/6-scale specimens with varying volumetric stirrup ratios and axial load levels, with specimen geometry and reinforcement layout illustrated in Figure 12. Jiang et al. (2024) performed similar tests on 1/10-scale specimens, considering variations in pier height, axial load ratio, longitudinal reinforcement ratio, and volumetric stirrup ratio. This section evaluates the applicability of the proposed ES model Equation 17 for round-ended hollow piers based on estimated ES values from 11 specimens in Shao et al. (2019) and Jiang et al. (2024). The key design parameters are summarized in Table 5, and the measured ES values were computed using the method proposed by Park (1989), as previously described.

Table 6 presents a comparison between the measured ES ratios (EI_{eff}/E_cI_g) and predictions from the Zheng model, the Wei model, and Equation 17. The results demonstrate that Equation 17 provides significantly better predictions, showing a mean ratio of calculated-to-measured ES of 0.976 with relative errors (RE) ranging from 4% to 21% (mean RE = 14%). In contrast, the Zheng and Wei models substantially overestimate the ES, yielding mean ratios of 1.510 (mean RE = 54%) and 1.225 (mean RE = 29%), respectively. This confirms the proposed model's superior accuracy for round-ended hollow piers compared to existing approaches.

However, Equation 17's predictions exhibit some variability, with a maximum RE of 21%, indicating notable sensitivity to certain parameters. Given the limited sample size, further experimental or numerical validation is recommended to better understand this sensitivity. Based on test conditions in Shao et al. (2019) and Jiang et al. (2024), the following parameter ranges are suggested for application of Equation 17 to round-ended hollow piers: a shear-span ratio of 2.5–6.5, a section hollowness ratio of 0.55–0.65, an axial load ratio of 0.05–0.15, and a straight segment length of section not exceeding the outer radius of the rounded ends.

8 Conclusion

This study evaluated ten existing ES models using a database of 50 CHRCP tests and identified key influencing factors through theoretical and experimental analyses. A new four-parameter model was proposed, incorporating axial load ratio, reinforcement ratio, shear-span ratio, and hollowness ratio. The model outperforms existing approaches in both accuracy and stability, with a mean stiffness ratio of 1.04 and a coefficient of variation of 0.21. It also shows good applicability to round-ended hollow piers. The results highlight the necessity of accounting for hollowness and shear effects in CHRCP design to avoid overestimating stiffness in seismic analysis. Within the investigated parameter ranges, the following key findings were obtained:

(1) Except for the Wei model, all existing ES models significantly overestimated the actual ES of CHRCPs on average, with predicted values ranging from 1.41 to 3.68 times the experimental values. The predictions of existing models exhibited considerable scatter, with coefficients of variation (COVs) ranging between 0.25 and 0.41. Among them, only the seismic code model had a COV of 0.25, while the others exceeded 0.32.

(2) Compared to existing models, the proposed model innovatively incorporates the influence of hollowness ratio and equivalent shear-span ratio on the ES of CHRCPs. Theoretical and experimental analyses revealed that the ES increases with axial load ratio, longitudinal reinforcement ratio, and shear-span ratio but decreases with hollowness ratio. The coupling effect of shear-span ratio and hollowness ratio can be accounted for by the equivalent shear-span ratio, with the ES increasing as the equivalent shear-span ratio increases.

(3) Among the existing models, the Zheng and Wei models provided relatively better predictions for the ES of CHRCPs, with mean ratios of calculated-to-measured stiffness of 1.42 and 0.90 and COVs of 0.32 and 0.36, respectively. The proposed model yielded predictions mostly between these two models, with a mean ratio of 1.04 and a COV of 0.21, demonstrating improved accuracy and reduced variability compared to existing models.

(4) The proposed model provides reliable estimates of the ES of CHRCPs. When combined with the Beam with Hinges element in OpenSees and an appropriate equivalent plastic hinge length, it accurately simulates the force–displacement hysteretic curves of full-scale and scaled CHRCPs under quasi-static loading.

(5) Although the proposed model outperforms existing models in predicting the ES of CHRCPs, it does not account for the interaction between longitudinal reinforcement ratio and axial load ratio, which slightly affects prediction accuracy. Additionally, due to experimental limitations, the database covers the following parameter ranges: an axial load ratio of 0.05–0.30, a longitudinal reinforcement ratio of 1.0%–5.4%, a hollowness ratio of 0.25–0.77, and a shear-span ratio of 2.5–6.1. For design parameters beyond these ranges—particularly for tall piers with shear-span ratios significantly exceeding 6—the ES may differ. Furthermore, the model does not consider the effects of soil–foundation interaction, concrete degradation, steel corrosion, or construction quality. Caution is advised when applying the proposed model to such scenarios, and appropriate modifications may be necessary.

(6) The proposed model is also applicable to rounded-ended hollow piers. Based on quasi-static test results from 11 such piers, the mean ratio of calculated-to-measured stiffness was 0.976, with a mean relative error of 14%, outperforming existing models. However, the key parameters of rounded-ended hollow piers must satisfy the following requirements: a shear-span ratio of 2.5–6.5, a section hollowness ratio of 0.55–0.65, an axial load ratio of 0.05–0.15, and a straight

segment length of section not exceeding the outer radius of the rounded ends.

Data availability statement

The raw data supporting the conclusions of this article will be made available by the authors, without undue reservation.

Author contributions

ZH: Writing – original draft, Writing – review and editing. GL: Writing – original draft, Writing – review and editing. WS: Investigation, Supervision, Writing – review and editing.

Funding

The author(s) declare that financial support was received for the research and/or publication of this article. The research for this manuscript was supported partially by the Project of Improving Basic Scientific Research Ability of Young and Middle-Aged Teachers in Guangxi Colleges and Universities (No. 2022KY1121).

Conflict of interest

Author ZH was employed by Guangxi Communications Design Group Co., Ltd.

The remaining authors declare that the research was conducted in the absence of any commercial or financial relationships that could be construed as a potential conflict of interest.

Generative AI statement

The author(s) declare that no Generative AI was used in the creation of this manuscript.

Publisher's note

References

AASHTO (2015). *Guide specifications for LRFD seismic bridge design*. Washington D.C.: American Association of State Highway and Transportation Officials.

ACI 318-19 (2019). *Building code requirements for structural concrete (ACI 318-19) and commentary*. Farmington Hills: American Concrete Institute.

ASCE 41-06 (2007). *Seismic rehabilitation of existing buildings*. Reston. doi:10.1061/9780784408841

Berry, M. P., Lehman, D. E., and Lowes, L. N. (2008). Lumped-plasticity models for performance simulation of bridge columns. *ACI Struct. J.* 105, 270–279. doi:10.14359/56427

Caltrans (2019). *Seismic design criteria (version 2.0)*. Sacramento: California Department of Transportation.

Chung, Y. S., Han, G. H., Lee, K. K., and Lee, D. H. (1999). Quasi-static test for seismic performance of circular hollow RC bridge pier. *J. Earthq. Eng. Soc. Korea* 3, 41–53. doi:10.22636/JKCI.1999.11.5.107

Elwood, K. J., and Eberhard, M. O. (2009). Effective stiffness of reinforced concrete columns. *ACI Struct. J.* 106, 476–484. doi:10.14359/56613

Eurocode 8 (2005). *Design provisions for earthquake resistance of structures - part 2: bridges*. Brussels: CEN.

FEMA 356 (2000). *Prestandard and commentary for the seismic rehabilitation of buildings*. Washington D.C.: Federal Emergency Management Agency.

Haselton, C. B., Liel, A. B., Lange, S. T., and Deierlein, G. G. (2008). "Beam-column element model calibrated for predicting flexural response leading to global collapse of RC FRame buildings," in *Report no. PEER-2007/03, Pacific earthquake engineering research center*. Berkeley.

Hoshikuma, J. I., and Priestley, M. J. N. (2000). *Flexural behavior of circular hollow columns with a single layer of reinforcement under seismic loading, report no. SSRP-2000/13*. San Diego: University of California.

Jiang, L. Z., Shao, G. Q., Wang, H., and Jiang, J. (2024). Experimental study on seismic performance of hollow piers with rounded rectangular cross section in high-speed railways. *Eng. Mech.* 31, 72–97. doi:10.6052/j.issn.1000-4750.2013.01.0111

JTG/T2231-01-2020 (2008). *Specifications for seismic design of highway bridges*. Beijing: China Communications Press.

Kim, T. H., and Kang, H. T. (2012). Seismic performance assessment of hollow circular reinforced concrete bridge columns with confinement steel. *J. Earthq. Eng. Soc. Korea* 16, 13–25. doi:10.5000/eesk.2012.16.1.013

Kim, T. H., Kim, H. Y., Lee, J. H., and Shin, H. M. (2016). New hollow RC bridge piers with triangular reinforcement details. *J. Earthq. Eng. Soc. Korea* 20, 21–31. doi:10.5000/eesk.2016.20.1.021

Kim, T. H., Lee, J. H., and Shin, H. M. (2014). Performance assessment of hollow RC bridge columns with triangular reinforcement details. *Mag. Concr. Res.* 66, 809–824. doi:10.1680/macr.13.00257

Kumar, R., and Singh, Y. (2010). Stiffness of reinforced concrete frame members for seismic analysis. *ACI Struct. J.* 107, 607–615. doi:10.14359/51663914

Kunnath, S. K., Heo, Y. A., and Mohle, J. F. (2009). Nonlinear uniaxial material model for reinforcing steel bars. *J. Struct. Eng.* 135, 335–343. doi:10.1061/(asce)0733-9445(2009)135:4(335)

Lee, J. H., Choi, J. H., Hwang, D. K., and Kwahk, I. J. (2015). Seismic performance of circular hollow RC bridge columns. *KSCE J. Civ. Eng.* 19, 1456–1467. doi:10.1007/s12205-014-1173-z

Li, G. Q., Tang, G. W., and Zheng, G. (2016). Equivalent plastic Hinge length of circular reinforced concrete bridge piers, China civ. *Eng. J.* 49, 87–97. doi:10.15951/j.tmgcxb.2016.02.010

Li, Z. X., Du, C. Y., Liang, X., and Zhao, B. (2020). Flexural behavior of circular hollow RC piers with reduced amounts of inner hoops. *Int. J. Concr. Struct. Mater.* 14, 9–15. doi:10.1186/s40069-019-0383-7

Liang, X., Du, C. Y., Zhao, B., and Li, Z. X. (2021b). Seismic performance of circular hollow concrete columns. *Struct. Concr.* 22, 3140–3155. doi:10.1002/suco.202000482

Liang, X., Du, C. Y., Zhao, B., Li, Z. X., Sritharan, S., and Zhang, H. D. (2021a). Performance of circular hollow concrete columns with a single layer of transverse reinforcement. *Struct* 32, 15–27. doi:10.1016/j.istruc.2021.02.051

Liang, X., and Sritharan, S. (2018). Effects of confinement in circular hollow concrete columns. *J. Struct. Eng.* 144, 04018159. doi:10.1061/(asce)st.1943-541x.0002151

Liang, X., and Sritharan, S. (2019). Effects of confinement in square hollow concrete column sections. *Eng. Struct.* 191, 526–535. doi:10.1016/j.engstruct.2019.04.034

Mander, J. B., Priestley, M. J. N., and Park, R. (1988). Theoretical stress-strain model for confined concrete. *J. Struct. Eng.* 114, 1804–1826. doi:10.1061/(asce)0733-9445(1988)114:8(1804)

OpenSees (2024). The open system for earthquake engineering simulation.

Park, R. (1989). Evaluation of ductility of structures and structural assemblages from laboratory testing. *Bullet N. Z. Soc. Earthq. Eng.* 22, 155–166. doi:10.5459/bnzsee.22.3.155-166

Paulay, T., and Priestley, M. J. N. (1992). *Seismic design of reinforced concrete and masonry buildings*. New York: John Wiley and Sons, Inc.

Priestley, M. J., Calvi, G. M., and Kowalsky, M. J. (2007). *Displacement based seismic design of structures*. Pavia: IUSS Press.

Ranzo, G., and Priestley, M. J. N. (2001). "Seismic performance of circular hollow columns subjected to high shear," in *Report no. SSRP-2001/01*. San Diego: University of California.

Scott, M. H., and Fenves, G. L. (2006). Plastic Hinge integration methods for force-based beam–column elements. *J. Struct. Eng.* 132, 244–252. doi:10.1061/(asce)0733-9445(2006)132:2(244)

Sezen, H., and Setzler, E. J. (2008). Reinforcement slip in reinforced concrete columns. *ACI Struct. J.* 105, 280–289. doi:10.14359/19787

Shao, C. J., Qi, Q. M., Wang, M., Xiao, Z. H., Wei, W., Hu, C. X., et al. (2019). Experimental study on the seismic performance of round-ended hollow piers. *Eng. Struct.* 195, 309–323. doi:10.1016/j.engstruct.2019.05.094

Sourav, D., and Satyabrata, C. (2020). Evaluation of effective stiffness of RC column sections by support vector regression approach. *Neural Comput. and Applic.* 32, 6997–7007. doi:10.1007/s00521-019-04190-0

Sun, Z. G., Wang, D. S., Li, H. N., and Traffic, J. (2013). Application of RC hollow bridge pier and review of seismic behavior research. *Transp. Eng.* 03, 22–32. doi:10.19818/j.cnki.1671-1637.2013.03.004

Unjoh, S., and Asazu, N. (1999). Strength and ductility characteristics of reinforced concrete column with circular hollow section, civ. *Eng. J.* 41, 60–65. doi:10.1061/JSDEAG.0005416

Wang, Z., Liu, T. X., Long, Z. L., Wang, J. Q., and Zhang, J. (2022). A machine-learning-based model for predicting the effective stiffness of precast concrete columns. *Eng. Struct.* 260, 114224. doi:10.1016/j.engstruct.2022.114224

Wang, Z., Wang, J. Q., Xiu, H. L., and Li, W. C. (2019). Equivalent plastic Hinge model of rectangular hollow piers. *China J. Highw. Transp.* 32, 76–86. doi:10.19721/j.cnki.1001-7372.2019.01.009

Wei, W., Shao, C. J., Xiao, Z. H., Qi, Q. M., Hu, C. X., Xiao, L. C., et al. (2019). Experimental study on effective stiffness of reinforced concrete hollow piers, China civ. *Eng. J.* 52, 105–114. doi:10.15951/j.tmgcxb.2019.10.008

Whittaker, D., Park, R., and Carr, A. J. (1987). "Experimental tests on hollow circular concrete columns for use in offshore concrete platforms," in *Proceedings of the 3rd Pacific conference on earthquake engineering* (New Zealand).

Yeh, Y. K., Mo, Y. L., and Yang, C. Y. (2001). Seismic performance of hollow circular bridge piers. *ACI Struct. J.* 98, 862–871. doi:10.1016/S0950-0618(02)00119-8

Yukio, M., Tadayosi, I., and Toshihiko, S. (1986). "Experimental study on deformation of circular cylindrical piers," in *The 7th proceedings of Japan earthquake engineering symposium, Japan*.

Zahn, F. A., Park, R., and Priestley, M. J. N. (1990). Flexural strength and ductility of circular hollow reinforced concrete columns without confinement on inside face. *ACI Struct. J.* 87, 156–166. doi:10.14359/9295

Zheng, G., and Li, G. Q. (2013). Effective stiffness of reinforced concrete bridge piers, China civ. *Eng. J.* 46, 44–52. doi:10.15951/j.tmgcxb.2013.06.004

Zhu, L. H., Bai, G. L., Li, X. W., Rong, Z., and Tu, F. (2009). Experimental study on seismic behavior of reinforced concrete pipe with a large cross section size and thinned wall. *Eng. Mech.* 26, 134–139.